

# Phased Array-Based Sub-Nyquist Sampling for Joint Wideband Spectrum Sensing and Direction-of-Arrival Estimation

Feiyu Wang, Jun Fang, Huiping Duan, and Hongbin Li, *Senior Member, IEEE*

**Abstract**—In this paper, we study the problem of joint wideband spectrum sensing and direction-of-arrival (DoA) estimation in a sub-Nyquist sampling framework. Specifically, considering a scenario where a few uncorrelated narrowband signals spread over a wide (say, several GHz) frequency band, our objective is to estimate the carrier frequencies and the DoAs associated with the narrowband sources, as well as reconstruct the power spectra of these narrowband signals. To overcome the sampling rate bottleneck for wideband spectrum sensing, we propose a new phased-array based sub-Nyquist sampling architecture with variable time delays, where a uniform linear array (ULA) is employed and the received signal at each antenna is delayed by a variable amount of time and then sampled by a synchronized low-rate analog-digital converter (ADC). Based on the collected sub-Nyquist samples, we calculate a set of cross-correlation matrices with different time lags, and develop a CANDECOMP/PARAFAC (CP) decomposition-based method for joint DoA, carrier frequency and power spectrum recovery. Perfect recovery conditions for the associated parameters and the power spectrum are analyzed. Our analysis reveals that our proposed method does not require to place any sparse constraint on the wideband spectrum, only needs the sampling rate to be greater than the bandwidth of the narrowband source signal with the largest bandwidth among all sources. Simulation results show that our proposed method can achieve an estimation accuracy close to the associated Cramér-Rao bounds (CRBs) using only a small number of data samples.

**Index Terms**—Joint wideband spectrum sensing and direction-of-arrival (DoA) estimation; compressed sensing; CANDECOMP/PARAFAC (CP) decomposition.

## I. INTRODUCTION

Wideband spectrum sensing, which aims to identify the frequency locations of a few narrowband transmissions that spread over a wide frequency band, has been of a growing interest in signal processing and cognitive radio communications [1], [2]. To perform wideband spectrum sensing, a conventional receiver requires to sample the received signal at the Nyquist rate, which may be infeasible if the spectrum under monitoring is very wide, say, reaches several GHz. Also,

a high sampling rate results in a large amount of data which place a heavy burden on subsequent storage and processing. To alleviate the sampling rate requirement, a variety of sub-Nyquist sampling schemes, e.g. [3]–[6], were developed. The rationale behind such schemes is to exploit the inherent sparsity in the frequency domain and formulate wideband spectrum sensing as a sparse signal recovery problem which, according to the compressed sensing theory [7], [8], can perfectly recover the signal of the entire frequency band based on compressed measurements or sub-Nyquist samples. Furthermore, in [9]–[11], it was shown that it is even possible to perfectly reconstruct the power spectrum without placing any sparse constraint on the wideband spectrum under monitoring.

In some applications such as electronic warfare, one need not only conduct wideband spectrum sensing, but also identify the carrier frequencies and directions-of-arrival (DoAs) associated with the narrowband signals that live within the wide frequency band [12]. Besides, in massive MIMO or millimeter wave systems where signals are transmitted via beamforming techniques, the DoA information would allow a cognitive radio to more efficiently exploit the vacant bands [13]. In [14], [15], ESPRIT-based methods were proposed for joint carrier frequency and DoA estimation. These methods, however, require the signal to be sampled at the Nyquist rate. Recently, with the advent of compressed sensing theories, the sparsity inherent in the spectral and spatial domains was utilized to devise sub-Nyquist sampling-based algorithms for joint wideband spectrum sensing and DoA estimation. Specifically, in [16], a compressed sensing method was developed in a phased array framework, where a multicoset sampling scheme is executed at each antenna to collect non-uniform samples. In practice, the multicoset sampling may be implemented using multiple channels, with each channel delayed by a different time offset and then sampled by a low-rate analog-digital converter (ADC). Since the multicoset sampling has to be performed at each antenna, the scheme [16] involves a high hardware complexity. In [17], [18], a simplified sub-Nyquist receiver architecture was proposed, in which each antenna output is connected with only two channels, i.e. a direct path and a delayed path. An ESPRIT-based algorithm was then developed for joint DoA, carrier frequency, and signal reconstruction. In addition to the above time delay-based sub-Nyquist receiver architectures, an alternative sub-Nyquist sampling approach, referred to as phased array-based modulated wideband converter (MWC), was proposed in [13], [19] for carrier and DoA estimation. The receiver utilizes an

Feiyu Wang, and Jun Fang are with the National Key Laboratory of Science and Technology on Communications, University of Electronic Science and Technology of China, Chengdu 611731, China, Email: JunFang@uestc.edu.cn

Huiping Duan is with the School of Electronic Engineering, University of Electronic Science and Technology of China, Chengdu 611731, China, Email: huipingduan@uestc.edu.cn

Hongbin Li is with the Department of Electrical and Computer Engineering, Stevens Institute of Technology, Hoboken, NJ 07030, USA, E-mail: Hongbin.Li@stevens.edu

This work was supported in part by the National Science Foundation of China under Grant 61522104, and the National Science Foundation under Grant ECCS-1408182 and Grant ECCS-1609393.

L-shaped array, and all sensors have the same sampling pattern implementing a single channel of the MWC. Perfect recovery conditions were analyzed, and reconstruction algorithms based on compressed sensing techniques were developed in [19].

In this paper, we propose a new sub-Nyquist receiver architecture, referred to as the phased-array based sub-Nyquist sampling architecture with variable time delays, for joint wide-band spectrum sensing and DoA estimation. Similar to [16]–[18], the proposed receiver architecture employs a uniform linear array. The received signal at each antenna is delayed by a pre-specified time shift and then sampled at a sub-Nyquist sampling rate. Compared with existing sub-Nyquist receiver architectures, our proposed sub-Nyquist scheme is simpler and easier to implement: it requires only one ADC for each antenna output, thus leading to a lower hardware complexity. Meanwhile, in our proposed architecture, the time delays for different antennas can be arbitrary as long as they satisfy a mild condition, which relaxes the requirement on the accuracy of time delay lines. From the collected sub-Nyquist samples, we calculate a set of cross-correlation matrices with different time lags, based on which a third-order tensor that admits a CANDECOMP/PARAFAC (CP) decomposition can be constructed. We show that the DoAs and the carrier frequencies, along with the power spectra associated with the sources, can be recovered from the factor matrices. The perfect recovery condition is analyzed. Our analysis shows that, to perfectly recover the power spectrum of the wide frequency band and the associated parameters, we only need the sampling rate to be greater than the bandwidth of the narrowband source signal with the largest bandwidth among all sources. In addition, our proposed method does not need to impose any sparse constraint on the wideband spectrum. We also derive the Cramér-Rao bound (CRB) results for our estimation problem. Simulation results show that our proposed method, with only a small number of data samples, can achieve an estimation accuracy close to the associated CRBs.

We notice that a CP decomposition-based approach was proposed in [13] for joint DoA and carrier frequency estimation. Different from our work, the construction of the tensor in [13] has to rely on an L-shaped array and exploits the cross-correlations between the two mutually perpendicular sub-arrays. In addition, the PARAFAC analysis in [13] can only help extract the DoA and carrier frequency information, while in our proposed method, the DoA, carrier frequency, and power spectrum associated with each source can be simultaneously recovered from the CP decomposition.

The rest of the paper is organized as follows. In Section II, we provide notations and basics on the CP decomposition. The signal model and related assumptions are discussed in Section III. In Section IV, we propose a new phase-array based sub-Nyquist receiver architecture. A CP decomposition-based method for joint wideband spectrum sensing and DoA estimation is developed in Section V. The uniqueness of the CP decomposition is discussed in Section VI, and the CRB analysis is conducted in Section VII. Simulation results are provided in Section VIII, followed by concluding remarks in Section IX.

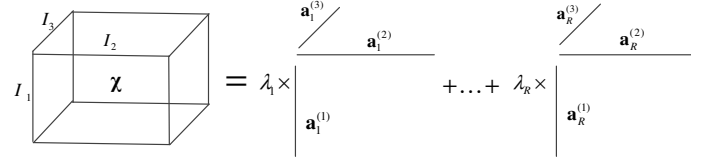


Fig. 1. Schematic of CP decomposition.

## II. PRELIMINARIES

To make the paper self-contained, we provide a brief review on tensors and the CP decomposition. More details regarding the notations and basics on tensors can be found in [20]. Simply speaking, a tensor is a generalization of a matrix to higher-order dimensions, also known as ways or modes. Vectors and matrices can be viewed as special cases of tensors with one and two modes, respectively. Throughout this paper, we use symbols  $\otimes$ ,  $\circ$ , and  $\odot$  to denote the Kronecker, outer, and Khatri-Rao product, respectively.

Let  $\mathcal{X} \in \mathbb{C}^{I_1 \times I_2 \times \dots \times I_N}$  denote an  $N$ th-order tensor with its  $(i_1, \dots, i_N)$ th entry denoted by  $\mathcal{X}_{i_1 \dots i_N}$ . Here the order  $N$  of a tensor is the number of dimensions. Fibers are higher-order analogues of matrix rows and columns. The mode- $n$  fibers of  $\mathcal{X}$  are  $I_n$ -dimensional vectors obtained by fixing every index but  $i_n$ . Slices are two-dimensional sections of a tensor, defined by fixing all but two indices. Unfolding or matricization is an operation that turns a tensor into a matrix. The mode- $n$  unfolding of a tensor  $\mathcal{X}$ , denoted as  $\mathbf{X}_{(n)}$ , arranges the mode- $n$  fibers to be the columns of the resulting matrix. The CP decomposition decomposes a tensor into a sum of rank-one component tensors (see Fig. 1), i.e.

$$\mathcal{X} = \sum_{r=1}^R \lambda_r \mathbf{a}_r^{(1)} \circ \mathbf{a}_r^{(2)} \circ \dots \circ \mathbf{a}_r^{(N)} \quad (1)$$

where  $\mathbf{a}_r^{(n)} \in \mathbb{C}^{I_n}$ , the minimum achievable  $R$  is referred to as the rank of the tensor, and  $\mathbf{A}^{(n)} \triangleq [\mathbf{a}_1^{(n)} \dots \mathbf{a}_R^{(n)}] \in \mathbb{C}^{I_n \times R}$  denotes the factor matrix along the  $n$ -th mode. Elementwise, we have

$$\mathcal{X}_{i_1 i_2 \dots i_N} = \sum_{r=1}^R \lambda_r a_{i_1 r}^{(1)} a_{i_2 r}^{(2)} \dots a_{i_N r}^{(N)} \quad (2)$$

The mode- $n$  unfolding of  $\mathcal{X}$  can be expressed as

$$\mathbf{X}_{(n)} = \mathbf{A}^{(n)} \mathbf{\Lambda} \left( \mathbf{A}^{(N)} \odot \dots \odot \mathbf{A}^{(n+1)} \odot \mathbf{A}^{(n-1)} \odot \dots \odot \mathbf{A}^{(1)} \right)^T \quad (3)$$

where  $\mathbf{\Lambda} \triangleq \text{diag}(\lambda_1, \dots, \lambda_R)$ .

## III. SIGNAL MODEL

Consider a scenario in which  $K$  uncorrelated, wide-sense stationary, and far-field narrowband signals spreading over a wide frequency band impinge on a wideband uniform linear array (ULA) with  $N$  receiver antennas, where we assume  $N > K$ . Let  $s(t)$  denote the combination of the  $K$  narrowband signals in the time domain.  $s(t)$  can be expressed as

$$s(t) = \sum_{k=1}^K s_k(t) e^{j\omega_k t} \quad (4)$$

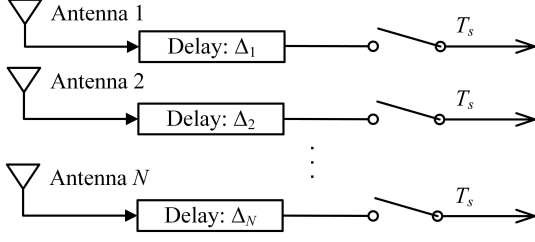


Fig. 2. Proposed Phased-Array based Sub-nyquist Sampling Architecture with variable Time delays (PASSAT).

where  $s_k(t)$  and  $\omega_k \in \mathbb{R}^+$  denote the complex baseband signal and the carrier frequency (in radians per second) of the  $k$ th source signal, respectively. Each source signal  $s_k(t)$  is associated with an unknown azimuth DoA  $\theta_k \in [0, \pi)$ . We have the following assumptions regarding the source signals:

- A1 The  $K$  source signals  $\{s_k(t)\}$  are assumed to be mutually uncorrelated, wide-sense stationary, and bandlimited to  $[-B/2, B/2]$ , i.e.  $B_k \leq B, \forall k$ , where  $B_k$  denotes the bandwidth of the  $k$ th source signal.
- A2 Sources either have distinct carrier frequencies  $\{\omega_k\}$  or distinct DoAs  $\{\theta_k\}$ , i.e. for any two source signals, we have  $(\theta_i, \omega_i) \neq (\theta_j, \omega_j), \forall i \neq j$ .
- A3 The multi-band signal  $s(t)$  is bandlimited to  $\mathcal{F} = [0, f_{\text{nyq}}]$ , and we assume  $f_{\text{nyq}} \gg B$ .

Assumption A2 is assumed to make signals distinguished from one another. Note that this assumption is less restrictive than the one made in other works, e.g. [17], [19], which, in order to remove the source ambiguity, require the quantity  $\omega_k \cos(\theta_k)$  to be mutually different for different signals, i.e.

$$\omega_i \cos(\theta_i) \neq \omega_j \cos(\theta_j) \quad \forall i \neq j \quad (5)$$

After collecting the received signal at the array, our objective is to jointly estimate the DoAs  $\{\theta_k\}$ , the carrier frequencies  $\{\omega_k\}$ , as well as the power spectra associated with the  $K$  source signals. To accomplish this task, we, in the following, propose a new phased-array based sub-Nyquist receiver architecture.

#### IV. PROPOSED SUB-NYQUIST RECEIVER ARCHITECTURE

##### A. Proposed Receiver Architecture

In our receiver architecture, the received signal at each antenna is delayed by a pre-specified factor  $\Delta_n$  and then sampled by a synchronous ADC with a sampling rate of  $f_s = 1/T_s$ , where  $f_s \ll f_{\text{nyq}}$ . We have the following assumptions regarding the delay factors and the sampling rate:

- A4 The time delay factors  $\{\Delta_n\}$  can take arbitrary values as long as the following condition holds valid

$$(\Delta_{n+2} - 2\Delta_{n+1} + \Delta_n)f_{\text{nyq}} < 1 \quad (6)$$

for some  $n \in \{1, \dots, N-2\}$ .

- A5 The sampling rate  $f_s$  is no less than the bandwidth of the narrowband source signal which has the largest bandwidth among all sources, i.e.  $f_s \geq B$ .

As will be shown later in our paper, Assumption A4 is essential to identify the unknown carrier frequencies. Also, in

practice, the time delay factors  $\{\Delta_n\}$  can be chosen to be of the same order of magnitude as the Nyquist sampling interval such that the narrowband approximation in (7) holds valid. The proposed receiver architecture, termed as the Phased-Array based Sub-Nyquist Sampling Architecture with variable Time delays (PASSAT), is illustrated in Fig. 2. The analog signal observed by the  $n$ th antenna can be expressed as

$$\begin{aligned} x_n(t) &= \sum_{k=1}^K s_k(t - (n-1)\tau_k - \Delta_n) \\ &\quad \times e^{j\omega_k(t - (n-1)\tau_k - \Delta_n)} + w_n(t) \\ &\approx \sum_{k=1}^K s_k(t) e^{j\omega_k(t - (n-1)\tau_k - \Delta_n)} + w_n(t) \end{aligned} \quad (7)$$

where the approximation is due to the narrowband assumption,  $w_n(t)$  represents the additive white Gaussian noise with zero mean and variance  $\sigma^2$ , and  $\tau_k$  denotes the delay between two adjacent sensors for a plane wave arriving in the direction  $\theta_k$  and is given by

$$\tau_k = \frac{d \cos \theta_k}{C} \quad (8)$$

Here  $d$  denotes the distance between two adjacent antennas and we assume

- A6 The distance between two adjacent antennas  $d$  satisfies  $d < C/f_{\text{nyq}}$ , where  $C$  is the speed of light.

We will show later that this assumption is essential for the recovery of the DoAs.

In practice, only the real part of  $x_n(t)$  is observed and sampled. Nevertheless, the corresponding imaginary part  $\Im[x_n(t)]$  can be retrieved from the real part  $\Re[x_n(t)]$  by passing the signal through a finite impulse response (FIR) Hilbert transformer. The complex analytic signal can also be roughly approximated by computing the discrete Fourier transform (DFT) of the output of each antenna and throwing away the negative frequency portion of the spectrum [12].

##### B. Relation to and Distinction from Existing Architectures

We notice that a time delay-based sub-Nyquist architecture was also introduced in [16]–[18]. Nevertheless, there are two key distinctions between our architecture and theirs. Firstly, our architecture has a simpler structure with only  $N$  delay channels, whereas the architecture proposed in [17] (see Fig. 3(a)) requires  $2N$  channels in total, in which each antenna output passes through two channels, namely, a direct path and a delayed path. As a consequence, the number of required ADCs for the architecture [17] is twice the number of ADCs for our architecture. In [18], a modified architecture was proposed based on [17]. It, however, still requires  $2N$  channels, with an  $N$ -channel delay network added to the first antenna. Secondly, for our proposed architecture, the time delays can take arbitrary values as long as the mild condition (6) is satisfied. In contrast, for other architectures, e.g. [16]–[18], a precise time control is required such that the time delays across different channels are strictly identical [17], [18], or the time delays must be integer multiples of the Nyquist sampling interval [16]. Due to the inaccuracy caused by the time shift

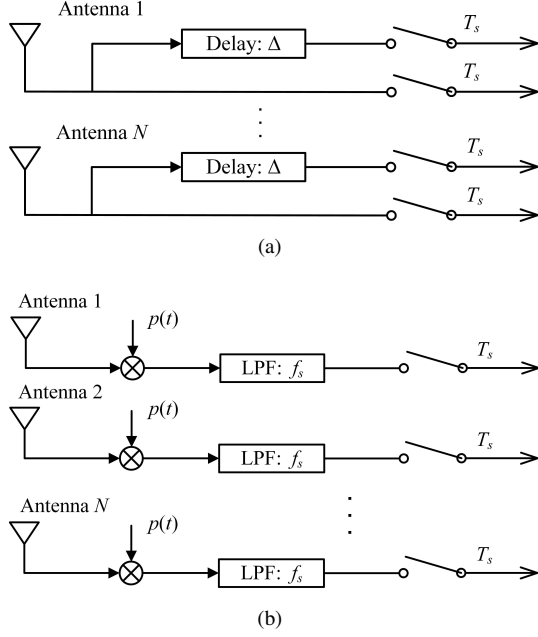


Fig. 3. Existing sub-Nyquist receiver architectures. (a) Sub-Nyquist sampling architecture proposed in [17]. (b) Sub-Nyquist sampling architecture proposed in [19].

elements, maintaining accurate time delays on the order of the Nyquist sampling interval is difficult. The inaccuracy in these delays will impair the recovery performance. Our architecture is free from this issue because it allows more flexible time delays and we can use the actual time delays measured in practice for our proposed recovery algorithm.

In [13], [19], a phased-array MWC-based sub-Nyquist sampling architecture (see Fig. 3(b)) was proposed for joint wideband spectrum sensing and DoA estimation, in which an L-shaped array composed of  $2N + 1$  sensors is adopted, and the output of each sensor is multiplied by a same periodic pseudo-random sequence, low-pass filtered and then sampled at a low rate. Compared to the phased-array MWC-based sub-Nyquist sampling architecture, our proposed delay-based scheme is much simpler to implement. In [21], it is argued that the delay-based architectures suffer two major disadvantages which include the need for high-precision delay lines as well as specialized ADCs with high analog bandwidth. Nevertheless, as discussed above, our proposed architecture, different from other delay-based schemes [16]–[18], has a relaxed requirement on the precision of delay lines. Regarding the latter issue, it is known that there is an inherent bandwidth limitation for practical ADCs, termed analog (full-power) bandwidth, which determines the highest frequency that can be handled by the device. In spite of that, we notice that the inherent bandwidth of some inexpensive, low-end commercial ADCs such as ADC12DC105 can reach up to 1GHz, while some high-end ADCs with affordable prices, such as ADC12D500, have an inherent bandwidth up to 2.7GHz, which may accommodate most wideband spectrum sensing applications.

## V. PROPOSED CP DECOMPOSITION-BASED METHOD

Let  $\delta(\cdot)$  denote the indicator function defined as

$$\delta(x) = \begin{cases} 1, & x = 0 \\ 0, & x \neq 0 \end{cases}. \quad (9)$$

We first calculate the cross-correlation between two sensor outputs  $x_m(t_1)$  and  $x_n(t_2)$ . Recalling Assumption A1, we have

$$\begin{aligned} R_{mn}^x(t_1, t_2) &= \mathbb{E}[x_m(t_1)x_n^*(t_2)] \\ &= \sum_{k=1}^K R_k^s(t_1, t_2)a_{mk}a_{nk}^* + R_{mn}^w(t_1, t_2) \end{aligned} \quad (10)$$

where

$$R_k^s(t_1, t_2) \triangleq \mathbb{E}[s_k(t_1)e^{j\omega_k t_1}s_k^*(t_2)e^{-j\omega_k t_2}] \quad (11)$$

denotes the autocorrelation of the  $k$ -th modulated source signal,

$$R_{mn}^w(t_1, t_2) \triangleq \mathbb{E}[w_m(t_1)w_n^*(t_2)] = \sigma^2\delta(m-n)\delta(t_1-t_2) \quad (12)$$

represents the autocorrelation of the additive noise and

$$a_{nk} \triangleq e^{-j((n-1)\tau_k\omega_k + \Delta_n\omega_k)} \quad (13)$$

Since the source signals are wide-sense stationary, the autocorrelation  $R_k^s(t_1, t_2)$  depends only on the time difference  $t_1 - t_2$ . As a result, the cross-correlation of the sensor outputs  $R_{mn}^x(t_1, t_2)$  depends on the time difference  $t_1 - t_2$  as well. Let  $T_s$  denote the sampling interval of the ADCs. The time difference has to be an integer multiple of the sampling interval, i.e.  $t_1 - t_2 = lT_s$  for  $l = -L, \dots, L$ . For notational convenience, we define

$$\begin{aligned} r_{m,n}^x(l) &\triangleq R_{mn}^x(t + lT_s, t) \\ r_k^s(l) &\triangleq R_k^s(t + lT_s, t) \\ r_{m,n}^w(l) &\triangleq R_{mn}^w(t + lT_s, t) \end{aligned}$$

We can therefore express (10) as a discrete-time form:

$$r_{m,n}^x(l) = \sum_{k=1}^K r_k^s(l)a_{mk}a_{nk}^* + r_{m,n}^w(l) \quad (14)$$

for  $l = -L, \dots, L$  and  $m, n = 1, \dots, N$ .

Our objective is to recover the DoAs  $\{\theta_k\}$ , the carrier frequencies  $\{\omega_k\}$ , as well as the power spectra associated with the  $K$  source signals based on the second-order statistics  $\{r_{m,n}^x(l)\}$ . For each time lag  $l$ , we can construct a correlation matrix  $\mathbf{R}^x(l)$  with its  $(m, n)$ th entry given by  $r_{m,n}^x(l)$ . Also, it can be easily verified that

$$\mathbf{R}^x(l) = \sum_{k=1}^K r_k^s(l)\mathbf{a}_k\mathbf{a}_k^H + \mathbf{R}^w(l) \quad (15)$$

where  $\mathbf{R}^w(l)$  denotes the cross-correlation matrix of the additive noise with its  $(m, n)$ th entry given by  $r_{m,n}^w(l)$ , and

$$\mathbf{a}_k \triangleq [a_{1k} \ a_{2k} \ \dots \ a_{Nk}]^T \quad (16)$$

Since a set of cross-correlation matrices  $\{\mathbf{R}^x(l)\}_{l=-L}^L$  are available, we can naturally express this set of correlation

matrices by a third-order tensor  $\mathcal{R}^x \in \mathbb{C}^{(2L-1) \times N \times N}$  whose three modes respectively stand for the time lag  $l$  and the antenna indices, and its  $(l, m, n)$ -th entry given by  $r_{m,n}^x(l)$ . Notice from (15) that each slice of the tensor  $\mathcal{R}^x$ ,  $\mathcal{R}^x(l)$ , is a weighted sum of a common set of rank-one outer products. The tensor  $\mathcal{R}^x$  thus admits a CP decomposition which decomposes a tensor into a sum of rank-one component tensors, i.e.

$$\mathcal{R}^x = \sum_{k=1}^K \mathbf{r}_k \circ \mathbf{a}_k \circ \mathbf{a}_k^* + \mathcal{R}^w \quad (17)$$

where  $\circ$  denotes the outer product,  $\mathcal{R}^w \in \mathbb{C}^{(2L-1) \times N \times N}$  with its  $(l, m, n)$ -th entry given by  $r_{m,n}^w(l)$ , and

$$\mathbf{r}_k \triangleq [r_k^s(-L) \ \dots \ r_k^s(L)]^T \quad (18)$$

Define

$$\mathbf{R} \triangleq [\mathbf{r}_1 \ \dots \ \mathbf{r}_K] \quad (19)$$

$$\mathbf{A} \triangleq [\mathbf{a}_1 \ \dots \ \mathbf{a}_K] \quad (20)$$

The three matrices  $\{\mathbf{R}, \mathbf{A}, \mathbf{A}^*\}$  are referred to as factor matrices associated with the noiseless version of  $\mathcal{R}^x$ . We see that the information about the parameters  $\{\theta_k, \omega_k\}$  as well as the power spectra can be extracted from the factor matrices. Motivated by this observation, we propose a two-stage method which consists of a CP decomposition stage whose objective is to estimate the factor matrices and a parameter estimation stage whose objective is to jointly recover the DoAs, carrier frequencies, and the power spectra of sources based on the estimated factor matrices.

#### A. CP Decomposition

We first consider the scenario where the number of sources,  $K$ , is known or estimated *a priori*. Clearly, the CP decomposition can be accomplished by solving the following optimization problem

$$\min_{\hat{\mathbf{R}}, \hat{\mathbf{A}}} \left\| \mathcal{R}^x - \sum_{k=1}^K \hat{\mathbf{r}}_k \circ \hat{\mathbf{a}}_k \circ \hat{\mathbf{a}}_k^* \right\|_F^2 \quad (21)$$

where  $\hat{\mathbf{R}} = [\hat{\mathbf{r}}_1 \ \dots \ \hat{\mathbf{r}}_K]$ ,  $\hat{\mathbf{A}} = [\hat{\mathbf{a}}_1 \ \dots \ \hat{\mathbf{a}}_K]$ , and  $\|\cdot\|_F$  denotes the Frobenius norm. On the other hand, note that the CP decomposition is unique under a mild condition. Therefore we can use a new variable  $\hat{\mathbf{b}}_k$  to replace  $\hat{\mathbf{a}}_k^*$ , which leads to

$$\min_{\hat{\mathbf{R}}, \hat{\mathbf{A}}, \hat{\mathbf{B}}} \left\| \mathcal{R}^x - \sum_{k=1}^K \hat{\mathbf{r}}_k \circ \hat{\mathbf{a}}_k \circ \hat{\mathbf{b}}_k \right\|_F^2 \quad (22)$$

where  $\hat{\mathbf{B}} \triangleq [\hat{\mathbf{b}}_1 \ \dots \ \hat{\mathbf{b}}_K]$ . The above optimization can be efficiently solved through an alternating least squares (ALS) procedure which alternatively updates one of the factor matrices to minimize the data fitting error while keeping the other

two factor matrices fixed:

$$\hat{\mathbf{R}}^{(t)} = \arg \min_{\mathbf{R}} \left\| (\mathbf{R}_{(1)}^x)^T - (\hat{\mathbf{B}}^{(t-1)} \odot \hat{\mathbf{A}}^{(t-1)}) \mathbf{R}^T \right\|_F^2 \quad (23)$$

$$\hat{\mathbf{A}}^{(t)} = \arg \min_{\mathbf{A}} \left\| (\mathbf{R}_{(2)}^x)^T - (\hat{\mathbf{B}}^{(t-1)} \odot \hat{\mathbf{R}}^{(t)}) \mathbf{A}^T \right\|_F^2 \quad (24)$$

$$\hat{\mathbf{B}}^{(t)} = \arg \min_{\mathbf{B}} \left\| (\mathbf{R}_{(3)}^x)^T - (\hat{\mathbf{A}}^{(t)} \odot \hat{\mathbf{R}}^{(t)}) \mathbf{B}^T \right\|_F^2 \quad (25)$$

where  $\mathbf{R}_{(n)}^x$  denotes the mode- $n$  unfolding of  $\mathcal{R}^x$ .

If the knowledge of the number of sources,  $K$ , is unavailable, more sophisticated CP decomposition techniques (e.g. [22]–[24]) can be employed to jointly estimate the model order and the factor matrices. The basic idea is to use low rank-promoting priors or functions to automatically determine the CP rank of the tensor. In [22], when the CP rank,  $K$ , is unknown, the following optimization was employed for CP decomposition

$$\begin{aligned} \min_{\hat{\mathbf{R}}, \hat{\mathbf{A}}, \hat{\mathbf{B}}} \quad & \|\mathcal{R}^x - \mathcal{X}\|_F^2 + \mu \left( \text{tr}(\hat{\mathbf{R}}\hat{\mathbf{R}}^H) + \text{tr}(\hat{\mathbf{A}}\hat{\mathbf{A}}^H) + \text{tr}(\hat{\mathbf{B}}\hat{\mathbf{B}}^H) \right) \\ \text{s.t.} \quad & \mathcal{X} = \sum_{k=1}^{\hat{K}} \hat{\mathbf{r}}_k \circ \hat{\mathbf{a}}_k \circ \hat{\mathbf{b}}_k \end{aligned} \quad (26)$$

where  $\hat{K} \gg K$  denotes an overestimated CP rank,  $\mu$  is a regularization parameter to control the tradeoff between low-rankness and the data fitting error,  $\hat{\mathbf{R}} = [\hat{\mathbf{r}}_1 \ \dots \ \hat{\mathbf{r}}_{\hat{K}}]$ ,  $\hat{\mathbf{A}} = [\hat{\mathbf{a}}_1 \ \dots \ \hat{\mathbf{a}}_{\hat{K}}]$ , and  $\hat{\mathbf{B}} = [\hat{\mathbf{b}}_1 \ \dots \ \hat{\mathbf{b}}_{\hat{K}}]$ . The above optimization (26) can still be solved by an ALS procedure as follows

$$\begin{aligned} \hat{\mathbf{R}}^{(t)} &= \arg \min_{\hat{\mathbf{R}}} \left\| \begin{bmatrix} (\mathbf{R}_{(1)}^x)^T \\ \mathbf{0} \end{bmatrix} - \begin{bmatrix} \hat{\mathbf{B}}^{(t-1)} \odot \hat{\mathbf{A}}^{(t-1)} \\ \sqrt{\mu} \mathbf{I} \end{bmatrix} \hat{\mathbf{R}}^T \right\|_F^2 \\ \hat{\mathbf{A}}^{(t)} &= \arg \min_{\hat{\mathbf{A}}} \left\| \begin{bmatrix} (\mathbf{R}_{(2)}^x)^T \\ \mathbf{0} \end{bmatrix} - \begin{bmatrix} \hat{\mathbf{B}}^{(t-1)} \odot \hat{\mathbf{R}}^{(t)} \\ \sqrt{\mu} \mathbf{I} \end{bmatrix} \hat{\mathbf{A}}^T \right\|_F^2 \\ \hat{\mathbf{B}}^{(t)} &= \arg \min_{\hat{\mathbf{B}}} \left\| \begin{bmatrix} (\mathbf{R}_{(3)}^x)^T \\ \mathbf{0} \end{bmatrix} - \begin{bmatrix} \hat{\mathbf{A}}^{(t)} \odot \hat{\mathbf{R}}^{(t)} \\ \sqrt{\mu} \mathbf{I} \end{bmatrix} \hat{\mathbf{B}}^T \right\|_F^2 \end{aligned}$$

The true CP rank of the tensor,  $K$ , can be estimated by removing those negligible rank-one tensor components after convergence.

#### B. Joint DoA, Carrier Frequency and Power Spectrum Estimation

We discuss how to jointly recover the DoAs, carrier frequencies, and power spectra of sources based on the estimated factor matrices. As shown in the next subsection, the CP decomposition is unique up to scaling and permutation ambiguities under a mild condition. More precisely, the estimated factor matrices and the true factor matrices are related as

$$\hat{\mathbf{R}} = \mathbf{R} \mathbf{\Lambda}_1 \mathbf{\Pi} + \mathbf{E}_1 \quad (27)$$

$$\hat{\mathbf{A}} = \mathbf{A} \mathbf{\Lambda}_2 \mathbf{\Pi} + \mathbf{E}_2 \quad (28)$$

$$\hat{\mathbf{B}} = \mathbf{A}^* \mathbf{\Lambda}_3 \mathbf{\Pi} + \mathbf{E}_3 \quad (29)$$

where  $\{\mathbf{\Lambda}_1, \mathbf{\Lambda}_2, \mathbf{\Lambda}_3\}$  are unknown nonsingular diagonal matrices which satisfy  $\mathbf{\Lambda}_1 \mathbf{\Lambda}_2 \mathbf{\Lambda}_3 = \mathbf{I}$ ;  $\mathbf{\Pi}$  is an unknown permutation matrix; and  $\mathbf{E}_1$ ,  $\mathbf{E}_2$ , and  $\mathbf{E}_3$  denote the estimation

errors associated with the three estimated factor matrices, respectively. The permutation matrix  $\mathbf{\Pi}$  can be ignored as it is common to all three factor matrices. Also, since we have prior knowledge that columns of  $\mathbf{A}/\sqrt{N}$  have unit norm, the amplitude ambiguity can be estimated and removed, in which case we can write

$$\hat{\mathbf{R}} = \mathbf{R}\tilde{\mathbf{\Lambda}}_1 + \tilde{\mathbf{E}}_1 \quad (30)$$

$$\hat{\mathbf{A}} = \mathbf{A}\tilde{\mathbf{\Lambda}}_2 + \tilde{\mathbf{E}}_2 \quad (31)$$

$$\hat{\mathbf{B}} = \mathbf{A}^* \tilde{\mathbf{\Lambda}}_3 + \tilde{\mathbf{E}}_3 \quad (32)$$

where  $\tilde{\mathbf{\Lambda}}_1, \tilde{\mathbf{\Lambda}}_2, \tilde{\mathbf{\Lambda}}_3$  are unknown nonsingular diagonal matrices with their diagonal elements lying on the unit circle.

Notice that the  $k$ th column of  $\mathbf{A}$  is characterized by the DoA and carrier frequency associated with the  $k$ th source. We now discuss how to estimate  $\{\omega_k\}$  and  $\{\tau_k\}$  from the estimated factor matrix  $\hat{\mathbf{A}}$ . Note that  $\hat{\mathbf{B}}$  is also an estimate of  $\mathbf{A}$ . Therefore either  $\hat{\mathbf{A}}$  or  $\hat{\mathbf{B}}$  can be used to estimate  $\{\omega_k\}$  and  $\{\tau_k\}$ . Let  $\hat{\mathbf{a}}_k$  denote the  $k$ -th column of  $\hat{\mathbf{A}}$ , and write

$$\tilde{\mathbf{\Lambda}}_2 = \text{diag}\{e^{-j\varphi_1}, \dots, e^{-j\varphi_K}\} \quad (33)$$

where  $\{\varphi_k\} \in [0, 2\pi)$  are unknown parameters. To simplify our exposition, we ignore the estimation errors  $\tilde{\mathbf{E}}_1, \tilde{\mathbf{E}}_2$ , and  $\tilde{\mathbf{E}}_3$ .

Write  $z = re^{j\varphi}$ , and define

$$\arg(z) \triangleq \text{mod}(\varphi, 2\pi) \quad \arg(z) \in [0, 2\pi) \quad (34)$$

where  $\text{mod}(a, b)$  is a modulo operator which returns the remainder of the Euclidean division of  $a$  by  $b$ . Recalling (13), we have

$$\begin{aligned} \eta_{nk} &\triangleq \text{mod}(-\arg(\hat{a}_{nk}), 2\pi) \\ &= \text{mod}((n-1)\tau_k\omega_k + \Delta_n\omega_k + \varphi_k, 2\pi) \end{aligned} \quad (35)$$

where  $\hat{a}_{nk}$  denotes the  $n$ th entry of  $\hat{\mathbf{a}}_k$ . Let

$$\boldsymbol{\eta}_k \triangleq [\eta_{1k} \ \dots \ \eta_{Nk}]^T$$

and let  $\mathbf{D}_p$  denote a difference matrix defined as

$$\mathbf{D}_p \triangleq \begin{pmatrix} -1 & 1 & 0 & \dots & 0 \\ 0 & -1 & 1 & \dots & 0 \\ \vdots & \vdots & \ddots & \ddots & \vdots \\ 0 & 0 & \dots & -1 & 1 \end{pmatrix} \in \mathbb{R}^{(p-1) \times p}$$

To recover  $\omega_k$ , we conduct a two-stage difference operation as follows

$$\boldsymbol{\beta}_k^{(1)} = \text{mod}(\mathbf{D}_N \boldsymbol{\eta}_k, 2\pi) \quad (36)$$

$$\boldsymbol{\beta}_k^{(2)} = \text{mod}(\mathbf{D}_{N-1} \boldsymbol{\beta}_k^{(1)}, 2\pi) \quad (37)$$

It can be easily verified that entries of  $\boldsymbol{\beta}_k^{(1)}$  and  $\boldsymbol{\beta}_k^{(2)}$  are respectively given as

$$\beta_{nk}^{(1)} = \text{mod}(\tau_k\omega_k + (\Delta_{n+1} - \Delta_n)\omega_k, 2\pi), \quad n = 1, \dots, N-1 \quad (38)$$

$$\beta_{nk}^{(2)} = \text{mod}((\Delta_{n+2} - 2\Delta_{n+1} + \Delta_n)\omega_k, 2\pi), \quad n = 1, \dots, N-2 \quad (39)$$

From (39), we can see that the information about the carrier frequency  $\omega_k$  is extracted after performing the two-stage difference operation. By properly devising the time delay factors  $\{\Delta_n\}$ , we can ensure that for some  $n_0 \in \{1, \dots, N\}$ , the condition (6) holds valid, i.e.

$$(\Delta_{n_0+2} - 2\Delta_{n_0+1} + \Delta_{n_0})f_{\text{nyq}} < 1 \quad (40)$$

The above condition implies

$$(\Delta_{n_0+2} - 2\Delta_{n_0+1} + \Delta_{n_0})\omega_{\max} < 2\pi \quad (41)$$

where  $\omega_{\max} \triangleq \max\{\omega_1, \dots, \omega_K\}$ . Therefore  $\omega_k$  can simply be estimated as

$$\hat{\omega}_k = \frac{\beta_{n_0,k}^{(2)}}{\Delta_{n_0+2} - 2\Delta_{n_0+1} + \Delta_{n_0}} \quad (42)$$

In fact, for a careful selection of time delay factors  $\{\Delta_n\}$ , the condition (6) (i.e. (40)) may be satisfied for different choices of  $n$ . As a result, we can obtain multiple estimates of  $\hat{\omega}_k$ . To improve the estimation performance, a final estimate of  $\hat{\omega}_k$  can be chosen as the average of these multiple estimates.

Under Assumption A6, that is,  $d < C/f_{\text{nyq}}$ , we have  $\tau_k\omega_{\max} < 2\pi$ . Thus, substituting the estimated  $\hat{\omega}_k$  back into (38),  $\tau_k$  can be obtained as

$$\hat{\tau}_k = \frac{\text{mod}(\beta_{nk}^{(1)} - (\Delta_{n+1} - \Delta_n)\hat{\omega}_k, 2\pi)}{\hat{\omega}_k} \quad (43)$$

Note that for each  $\beta_{nk}^{(1)}, n = 1, \dots, N-1$ , we can obtain an estimate of  $\tau_k$ . Therefore multiple estimates of  $\tau_k$  can be collected. Again, an average operation can be conducted to yield a final estimate of  $\tau_k$ . Based on  $\hat{\tau}_k$ , an estimate of the associated DoA  $\theta_k$  can be readily obtained from (8).

We now discuss how to recover the power spectra of the sources  $\{s_k(t)\}$ . Let  $\tilde{r}_k^s(\tau) \triangleq R_k^s(t + \tau, t)$ , where  $\tau \in \mathbb{R}$  can be any real value. The power spectrum of the  $k$ th source can thus be expressed as the Fourier transform of  $\tilde{r}_k^s(\tau)$ , i.e.

$$\tilde{S}_k(\omega) = \int_{-\infty}^{+\infty} \tilde{r}_k^s(\tau) e^{-j\omega\tau} d\tau \quad (44)$$

Let  $S_k(\omega)$  denote the discrete-time Fourier transform (DTFT) of the autocorrelation sequence  $\{r_k^s(l)\}_{l=-\infty}^{+\infty}$ , i.e.

$$S_k(\omega) = \sum_{l=-\infty}^{\infty} r_k^s(l) e^{-j\omega l T_s} \quad (45)$$

According to the sampling theorem,  $\tilde{S}_k(\omega)$  and  $S_k(\omega)$  are related as follows

$$S_k(\omega) = \frac{1}{T_s} \sum_{n=-\infty}^{+\infty} \tilde{S}_k\left(\omega + n\frac{2\pi}{T_s}\right) \quad (46)$$

Under Assumption A5, i.e.  $f_s \geq B \geq B_k$ , the power spectrum  $\tilde{S}_k(\omega)$  can be perfectly recovered by filtering  $S_k(\omega)$  with a bandpass filter, i.e.

$$\tilde{S}_k(\omega) = \begin{cases} T_s S_k(\omega), & \omega \in [\omega_k - \pi f_s, \omega_k + \pi f_s] \\ 0, & \omega \notin [\omega_k - \pi f_s, \omega_k + \pi f_s] \end{cases} \quad (47)$$

Given the estimated factor matrix  $\hat{\mathbf{R}}$ , the DTFT of the autocorrelation sequence  $\{r_k^s(l)\}$  can be approximated as

$$\hat{S}_k(\omega) = \sum_{l=-L}^L \hat{r}_k^s(l) e^{-j\omega l T_s} \quad (48)$$

When  $L$  is chosen to be sufficiently large, the estimation error due to the time lag truncation is negligible. Also, although there exists a phase ambiguity between the estimated autocorrelation sequence  $\hat{r}_k$  and the true autocorrelation sequence  $r_k$ , this phase ambiguity can be removed by noting that the power spectrum  $S_k(\omega)$  is real and non-negative. In addition, the power spectrum of each source is automatically paired with its associated DoA and carrier frequency due to the reason that both  $\hat{\mathbf{R}}$  and  $\hat{\mathbf{A}}$  experience a common permutation operation.

## VI. UNIQUENESS OF CP DECOMPOSITION

We see that the uniqueness of the CP decomposition is crucial to our proposed method. It is well known that the essential uniqueness of CP decomposition can be guaranteed by Kruskal's condition [25]. Let  $k_{\mathbf{X}}$  denote the k-rank of a matrix  $\mathbf{X}$ , which is defined as the largest value of  $k_{\mathbf{X}}$  such that every subset of  $k_{\mathbf{X}}$  columns of the matrix  $\mathbf{X}$  is linearly independent. We have the following theorem concerning the uniqueness of CP decomposition.

*Theorem 1:* Let  $(\mathbf{X}, \mathbf{Y}, \mathbf{Z})$  be a CP solution which decomposes a third-order tensor  $\mathcal{X} \in \mathbb{C}^{d_1 \times d_2 \times d_3}$  into  $p$  rank-one arrays, where  $\mathbf{X} \in \mathbb{C}^{d_1 \times p}$ ,  $\mathbf{Y} \in \mathbb{C}^{d_2 \times p}$ , and  $\mathbf{Z} \in \mathbb{C}^{d_3 \times p}$ . Suppose the following Kruskal's condition

$$k_{\mathbf{X}} + k_{\mathbf{Y}} + k_{\mathbf{Z}} \geq 2p + 2 \quad (49)$$

holds and there is an alternative CP solution  $(\hat{\mathbf{X}}, \hat{\mathbf{Y}}, \hat{\mathbf{Z}})$  which also decomposes  $\mathcal{X}$  into  $p$  rank-one arrays. Then we have  $\hat{\mathbf{X}} = \mathbf{X} \mathbf{\Pi} \mathbf{\Lambda}_x$ ,  $\hat{\mathbf{Y}} = \mathbf{Y} \mathbf{\Pi} \mathbf{\Lambda}_y$ , and  $\hat{\mathbf{Z}} = \mathbf{Z} \mathbf{\Pi} \mathbf{\Lambda}_z$ , where  $\mathbf{\Pi}$  is a unique permutation matrix and  $\mathbf{\Lambda}_x$ ,  $\mathbf{\Lambda}_y$ , and  $\mathbf{\Lambda}_z$  are unique diagonal matrices such that  $\mathbf{\Lambda}_x \mathbf{\Lambda}_y \mathbf{\Lambda}_z = \mathbf{I}$ .

*Proof:* A rigorous proof can be found in [26]. ■

Note that Kruskal's condition cannot hold when  $R = 1$ . However, in that case the uniqueness has been proven by Harshman [27]. Kruskal's sufficient condition is also necessary for  $R = 2$  and  $R = 3$ , but not for  $R > 3$  [26].

From the above theorem, we know that if

$$k_{\mathbf{R}} + k_{\mathbf{A}} + k_{\mathbf{A}^*} \geq 2K + 2 \quad (50)$$

then the CP decomposition of  $\mathcal{R}^x$  is essentially unique. Since  $\mathbf{A}^*$  is the complex conjugate of  $\mathbf{A}$ , we only need to examine the k-ranks of  $\mathbf{A}$  and  $\mathbf{R}$ .

Note that the  $(n, k)$ th entry of  $\mathbf{A}$  is given by

$$a_{nk} = e^{-j((n-1)\tau_k \omega_k + \Delta_n \omega_k)} \quad (51)$$

which is a function of the time delay factor  $\Delta_n$ . It is not difficult to design a set of time delay factors  $\{\Delta_n\}$  such that  $k_{\mathbf{A}} = K$ . For example, we divide  $N$  antennas into two groups  $S_1 = \{1, \dots, K\}$  and  $S_2 = \{K+1, \dots, N\}$ . We set the delay factors in the first group to be linearly proportional to  $n-1$ , i.e.  $\Delta_n = (n-1)\nu$  for  $n \in S_1$ , where  $\nu \geq 0$  is a constant. In this case, the first  $K$  rows of  $\mathbf{A}$  form a Vandermonde matrix:

$$\mathbf{A}_{[1:K,:]} = \text{Vand}(\tau_1 \omega_1 + \nu \omega_1, \dots, \tau_K \omega_K + \nu \omega_K) \quad (52)$$

where  $\text{Vand}(\phi_1, \dots, \phi_K)$  is defined as

$$\text{Vand}(\phi_1, \dots, \phi_K) \triangleq \begin{bmatrix} e^{-j(0\phi_1)} & \dots & e^{-j(0\phi_K)} \\ e^{-j(1\phi_1)} & \dots & e^{-j(1\phi_K)} \\ \vdots & \ddots & \vdots \\ e^{-j((K-1)\phi_1)} & \dots & e^{-j((K-1)\phi_K)} \end{bmatrix}$$

Thus  $\mathbf{A}$  is full column rank with  $k_{\mathbf{A}} = K$  as long as  $\{\omega_k \tau_k + \nu \omega_k\}$  are distinct from each other. If we set  $\nu = 0$ , we only need  $\{\omega_k \tau_k\}$ , i.e.  $\{\omega_k \cos \theta_k\}$ , are distinct from each other. For the case where the quantities  $\{\omega_k \cos \theta_k\}$  for different source signals may be identical, we can set  $\nu \neq 0$ , in which case we still have  $k_{\mathbf{A}} = K$  provided that the carrier frequencies  $\{\omega_k\}$  are mutually different. In other words, as long as Assumption A2 is satisfied, we can always set an appropriate value of  $\nu$  to ensure  $k_{\mathbf{A}} = K$ . For other more general choices of time delay factors  $\{\Delta_n\}$ , it can be numerically checked that the k-rank of  $\mathbf{A}$  still equals to  $K$  with a high probability, although a rigorous proof is difficult.

Since we have  $k_{\mathbf{A}} = K$ , we only need  $k_{\mathbf{R}} \geq 2$  in order to satisfy Kruskal's condition. This condition  $k_{\mathbf{R}} \geq 2$  is met if every two columns of  $\mathbf{R}$  are linearly independent. Note that the  $k$ th column of  $\mathbf{R}$ ,  $\mathbf{r}_k$ , is a truncated autocorrelation sequence of the  $k$ th modulated signal  $s_k(t)e^{j\omega_k t}$ . Clearly, if the baseband signals  $\{s_k(t)\}$  have distinct power spectra, then any two columns of  $\mathbf{R}$  are linearly independent, which implies  $k_{\mathbf{R}} \geq 2$ . In practice, since source signals usually have different bandwidths, the diverse power spectra condition can be easily satisfied. Even if the baseband signals  $\{s_k(t)\}$  have identical power spectra, the autocorrelation sequences of any two modulated signals  $\{s_{k_1}(t)e^{j\omega_{k_1} t}, s_{k_2}(t)e^{j\omega_{k_2} t}\}$  could still be linearly independent as long as their carrier frequencies satisfy

$$\text{mod}\{|\omega_{k_1} - \omega_{k_2}|, 2\pi f_s\} \neq 0 \quad (53)$$

The above condition ensures that autocorrelation sequences  $\{\mathbf{r}_k\}$  of different modulated signals have distinct exponential terms  $\{e^{j\omega_k l T_s}\}$  (see (11)). Due to the randomness of locations of the carrier frequencies, the condition (53) is very likely to be satisfied in practice. As a result, we have  $k_{\mathbf{R}} \geq 2$ .

## VII. CRB ANALYSIS

In this section, we develop Cramér-Rao bound (CRB) results for the joint DoA, carrier frequency, and power spectra estimation problem considered in this paper. As is well known, the CRB is a lower bound on the variance of any unbiased estimator [28]. It provides a benchmark for evaluating the performance of our proposed method. In addition, the CRB results illustrate the behavior of the resulting bounds, which helps understand the effect of different system parameters, including the noise power  $\sigma^2$ , the number of antennas  $N$  and the number of samples  $N_s$ , on the estimation performance.

### A. Signal Model

Recall that the analog signal at each antenna is sampled with a sampling rate  $f_s = 1/T_s$ . The sampled signal at the

$n$ th antenna can be written as (cf. (7))

$$\begin{aligned} x_n(lT_s) &= \sum_{k=1}^K s_k(lT_s) e^{j\omega_k(lT_s - (n-1)\tau_k - \Delta_n)} + w_n(lT_s) \\ &= \sum_{k=1}^K a_{nk} s_k(lT_s) e^{j\omega_k(lT_s)} + w_n(lT_s) \end{aligned} \quad (54)$$

The above signal model can be rewritten in a vector-matrix form as

$$\mathbf{x}_l = \mathbf{A} \mathbf{s}_l + \mathbf{w}_l, \quad l = 0, \dots, N_s - 1 \quad (55)$$

where  $\mathbf{A}$  is defined in (20),  $\mathbf{x}_l \triangleq [x_1(lT_s) \dots x_N(lT_s)]^T$ ,  $\mathbf{w}_l \triangleq [w_1(lT_s) \dots w_N(lT_s)]^T$ , and

$$\mathbf{s}_l \triangleq [s_1(lT_s) e^{j\omega_1(lT_s)} \dots s_K(lT_s) e^{j\omega_K(lT_s)}]^T$$

Suppose we collect a total number of  $N_s$  ( $l = 0, \dots, N_s - 1$ ) samples. The received signal can thus be expressed as

$$\mathbf{X} = \mathbf{A} \mathbf{S} + \mathbf{W} \quad (56)$$

where

$$\begin{aligned} \mathbf{X} &\triangleq [\mathbf{x}_0 \dots \mathbf{x}_{N_s-1}] \\ \mathbf{S} &\triangleq [\mathbf{s}_0 \dots \mathbf{s}_{N_s-1}] \\ \mathbf{W} &\triangleq [\mathbf{w}_0 \dots \mathbf{w}_{N_s-1}]. \end{aligned}$$

Let  $\mathbf{x} \triangleq \text{vec}(\mathbf{X}^T)$ , where  $\text{vec}(\mathbf{Z})$  denotes a vectorization operation which stacks the columns of  $\mathbf{Z}$  into a single column vector. We have

$$\mathbf{x} = \bar{\mathbf{A}} \mathbf{s} + \mathbf{w} \quad (57)$$

where

$$\begin{aligned} \mathbf{x} &\triangleq \text{vec}(\mathbf{X}^T), \quad \mathbf{w} \triangleq \text{vec}(\mathbf{W}^T) \\ \mathbf{s} &\triangleq \text{vec}(\mathbf{S}^T), \quad \bar{\mathbf{A}} \triangleq \mathbf{A} \otimes \mathbf{I}_{N_s} \end{aligned} \quad (58)$$

in which  $\mathbf{I}_n$  denotes an  $n \times n$  identity matrix. We assume that  $\mathbf{w} \sim \mathcal{CN}(\mathbf{0}, \sigma^2 \mathbf{I}_{N \cdot N_s})$  and  $\mathbf{s} \sim \mathcal{CN}(\mathbf{0}, \mathbf{R}_s)$  follow a circularly-symmetric complex Gaussian distribution, where  $\mathbf{R}_s$  denotes the source covariance matrix which needs to be estimated along with other parameters. Note that in our proposed algorithm, the additive noise  $\mathbf{w}$  and the source signal  $\mathbf{s}$  are not restricted to be circularly-symmetric complex Gaussian. Here we make such an assumption in order to facilitate the CRB analysis.

Under the assumption that  $\mathbf{w}$  and  $\mathbf{s}$  are circularly-symmetric complex Gaussian random variables, we can readily verify that  $\mathbf{x}$  also follows a circularly-symmetric complex Gaussian distribution, i.e.  $\mathbf{x} \sim \mathcal{CN}(\mathbf{0}, \mathbf{R}_x)$ , where

$$\begin{aligned} \mathbf{R}_x &\triangleq \mathbb{E}[\mathbf{x} \mathbf{x}^H] = \mathbb{E}[\bar{\mathbf{A}} \mathbf{s} \mathbf{s}^H \bar{\mathbf{A}}^H] + \mathbb{E}[\mathbf{w} \mathbf{w}^H] \\ &= \bar{\mathbf{A}} \mathbf{R}_s \bar{\mathbf{A}}^H + \sigma^2 \mathbf{I}_{N \cdot N_s} \end{aligned} \quad (59)$$

From Assumption A1, we know that  $\mathbf{R}_s$  is a block diagonal matrix, i.e.

$$\mathbf{R}_s = \text{diag}(\mathbf{P}_1, \dots, \mathbf{P}_K). \quad (60)$$

where  $\mathbf{P}_k \triangleq \mathbb{E}[\tilde{\mathbf{s}}_k \tilde{\mathbf{s}}_k^H]$  denotes the autocorrelation matrix of the  $k$ th signal, and  $\tilde{\mathbf{s}}_k$  is the transpose of the  $k$ th row of  $\mathbf{S}$ , i.e.

$$\tilde{\mathbf{s}}_k \triangleq [s_k(0T_s) e^{j\omega_k(0T_s)} \dots s_k((N_s - 1)T_s) e^{j\omega_k((N_s - 1)T_s)}]^T$$

Also, in Assumption A1, each source is assumed to be wide-sense stationary. Therefore the autocorrelation matrix  $\mathbf{P}_k$  is a Hermitian-Toeplitz matrix. Here Toeplitz means that it has diagonal-constant entries, i.e. each descending diagonal from left to right is constant. Let  $p_0^k$  denote the constant for elements located on the main diagonal, and  $p_l^k$ ,  $l \geq 1$ , denote the constant for elements located on the  $l$ th diagonal below the main diagonal of  $\mathbf{P}_k$ . Let

$$\mathbf{T}_l \triangleq \begin{pmatrix} \mathbf{0} & \mathbf{I}_{N_s-l} \\ \mathbf{0} & \mathbf{0} \end{pmatrix} \in \mathbb{R}^{N_s \times N_s}$$

and

$$\mathbf{T}_{-l} \triangleq \begin{pmatrix} \mathbf{0} & \mathbf{0} \\ \mathbf{I}_{N_s-l} & \mathbf{0} \end{pmatrix} \in \mathbb{R}^{N_s \times N_s}$$

The autocorrelation matrix  $\mathbf{P}_k$  can thus be expressed as

$$\mathbf{P}_k = p_0^k \mathbf{I}_{N_s} + \sum_{l=1}^L [p_l^k \mathbf{T}_{-l} + (p_l^k)^* \mathbf{T}_l] \quad (61)$$

where  $L$  is chosen to be sufficiently large to ensure  $p_l^k = 0$  for  $l > L$ . From (61), we can see that  $\mathbf{P}_k$  is characterized by parameters

$$\mathbf{p}_k \triangleq [p_0^k \Re(p_1^k) \dots \Re(p_L^k) \Im(p_1^k) \dots \Im(p_L^k)] \quad (62)$$

As a result,  $\mathbf{R}_s$  is characterized by parameters

$$\mathbf{p} \triangleq [\mathbf{p}_1 \dots \mathbf{p}_K] \quad (63)$$

On the other hand, notice that  $\bar{\mathbf{A}}$  is a parameterized matrix, with each column of  $\bar{\mathbf{A}}$  determined by the DoA and the carrier frequency of each source, i.e.  $\{\theta_k, \omega_k\}$ . Unfortunately, the value ranges for the DoA and the carrier frequency differ by orders of magnitude, which may cause numerical instability in computing the CRB matrix. To address this difficulty, we, instead, analyze the CRB for the following two parameters  $\{\xi_k, \psi_k\}$  defined as

$$\xi_k \triangleq \omega_k \tau_k \quad \psi_k \triangleq \omega_k / c \quad (64)$$

where  $c$  is a parameter appropriate chosen (e.g.  $c = 10^9$ ) such that values of  $\xi_k$  and  $\psi_k$  roughly have the same scale. Also, we define

$$\begin{aligned} \boldsymbol{\xi} &\triangleq [\xi_1 \dots \xi_K] \\ \boldsymbol{\psi} &\triangleq [\psi_1 \dots \psi_K] \end{aligned}$$

We see that the complete set of parameters to be estimated include

$$\boldsymbol{\alpha} \triangleq [\boldsymbol{\xi} \ \boldsymbol{\psi} \ \mathbf{p} \ \sigma^2] \quad (65)$$

Recall that  $\mathbf{x}$  follows a complex Gaussian distribution with zero mean and covariance matrix  $\mathbf{R}_x$ . Therefore the log-likelihood function of  $\boldsymbol{\alpha}$  can be expressed as

$$L(\boldsymbol{\alpha}) \propto -\ln |\mathbf{R}_x| - \mathbf{x}^H \mathbf{R}_x^{-1} \mathbf{x} \quad (66)$$



### B. Calculation of The CRB Matrix

Since the random vector  $\mathbf{x}$  follows a circularly-symmetric complex Gaussian distribution, we can resort to the Slepian-Bangs formula [29], [30] to compute the Fisher information matrix (FIM). According to the Slepian-Bangs formula, the  $(i, j)$ th element of the FIM  $\mathbf{\Omega}$  is calculated as

$$\Omega_{ij} = \text{tr} \left( \mathbf{R}_x^{-1} \frac{\partial \mathbf{R}_x}{\partial \alpha_i} \mathbf{R}_x^{-1} \frac{\partial \mathbf{R}_x}{\partial \alpha_j} \right) \quad (67)$$

where  $\alpha_i$  and  $\alpha_j$  denote the  $i$ th and the  $j$ th entries of  $\boldsymbol{\alpha}$ , respectively.

By utilizing the structures of  $\bar{\mathbf{A}}$  and  $\mathbf{R}_s$  (cf. (58) and (60)),  $\mathbf{R}_x$  can be expressed as

$$\begin{aligned} \mathbf{R}_x &= [\mathbf{a}_1 \otimes \mathbf{I}_{N_s} \ \dots \ \mathbf{a}_K \otimes \mathbf{I}_{N_s}] \cdot \text{diag}(\mathbf{P}_1, \dots, \mathbf{P}_K) \\ &\quad \cdot [\mathbf{a}_1 \otimes \mathbf{I}_{N_s} \ \dots \ \mathbf{a}_K \otimes \mathbf{I}_{N_s}]^H + \sigma^2 \mathbf{I}_{N \cdot N_s} \\ &= [\mathbf{a}_1 \otimes \mathbf{P}_1 \ \dots \ \mathbf{a}_K \otimes \mathbf{P}_K] \\ &\quad \cdot [\mathbf{a}_1 \otimes \mathbf{I}_{N_s} \ \dots \ \mathbf{a}_K \otimes \mathbf{I}_{N_s}]^H + \sigma^2 \mathbf{I}_{N \cdot N_s} \\ &= \sum_{k=1}^K (\mathbf{a}_k \mathbf{a}_k^H) \otimes \mathbf{P}_k + \sigma^2 \mathbf{I}_{N \cdot N_s} \end{aligned} \quad (68)$$

where  $\mathbf{a}_k$ , defined in (16), is the  $k$ th column of  $\mathbf{A}$ .

We first compute the partial derivative of  $\mathbf{R}_x$  with respect to  $\xi_k$  and  $\psi_k$ . From (13) and the definition of  $\{\xi_k, \psi_k\}$ , we can write

$$a_{nk} = e^{-j((n-1)\xi_k + c\Delta_n\psi_k)} \quad (69)$$

Thus we have

$$\frac{\partial \mathbf{a}_k}{\partial \xi_k} = -j \cdot \text{diag}(0, \dots, N-1) \cdot \mathbf{a}_k \quad (70)$$

$$\frac{\partial \mathbf{a}_k}{\partial \psi_k} = -j \cdot c \cdot \text{diag}(\Delta_1, \dots, \Delta_N) \cdot \mathbf{a}_k \quad (71)$$

Combining (68) and (70)–(71), we have

$$\frac{\partial \mathbf{R}_x}{\partial \xi_k} = \left( \frac{\partial \mathbf{a}_k}{\partial \xi_k} \mathbf{a}_k^H + \mathbf{a}_k \frac{\partial \mathbf{a}_k^H}{\partial \xi_k} \right) \otimes \mathbf{P}_k \quad (72)$$

$$\frac{\partial \mathbf{R}_x}{\partial \psi_k} = \left( \frac{\partial \mathbf{a}_k}{\partial \psi_k} \mathbf{a}_k^H + \mathbf{a}_k \frac{\partial \mathbf{a}_k^H}{\partial \psi_k} \right) \otimes \mathbf{P}_k. \quad (73)$$

Similarly, we can obtain the partial derivatives with respect to other parameters as follows

$$\begin{aligned} \frac{\partial \mathbf{R}_x}{\partial (p_0^k)} &= (\mathbf{a}_k \mathbf{a}_k^H) \otimes \left( \frac{\partial \mathbf{P}_k}{\partial (p_0^k)} \right) \\ &= (\mathbf{a}_k \mathbf{a}_k^H) \otimes \mathbf{I}_{N_s} \end{aligned} \quad (74)$$

$$\begin{aligned} \frac{\partial \mathbf{R}_x}{\partial (\Re(p_l^k))} &= (\mathbf{a}_k \mathbf{a}_k^H) \otimes \left( \frac{\partial \mathbf{P}_k}{\partial (\Re(p_l^k))} \right) \\ &= (\mathbf{a}_k \mathbf{a}_k^H) \otimes (\mathbf{T}_{-l} + \mathbf{T}_l) \end{aligned} \quad (75)$$

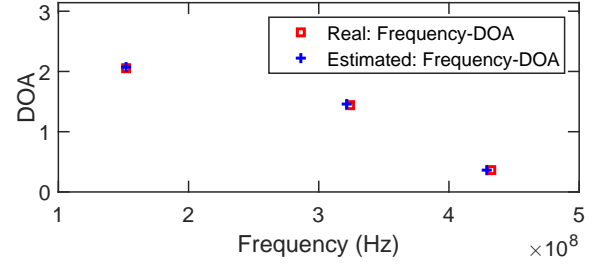
$$\begin{aligned} \frac{\partial \mathbf{R}_x}{\partial (\Im(p_l^k))} &= (\mathbf{a}_k \mathbf{a}_k^H) \otimes \left( \frac{\partial \mathbf{P}_k}{\partial (\Im(p_l^k))} \right) \\ &= (\mathbf{a}_k \mathbf{a}_k^H) \otimes (j\mathbf{T}_{-l} - j\mathbf{T}_l) \end{aligned} \quad (76)$$

and

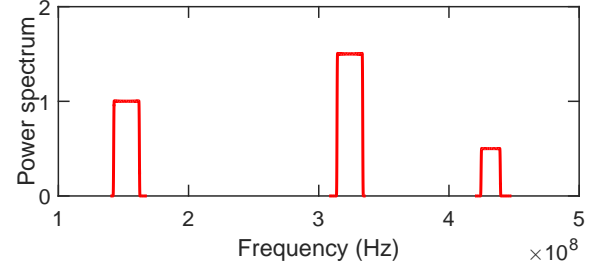
$$\frac{\partial \mathbf{R}_x}{\partial (\sigma^2)} = \mathbf{I}_{N \cdot N_s}. \quad (77)$$

After obtaining the FIM  $\mathbf{\Omega}$ , the CRB can be calculated as [28]

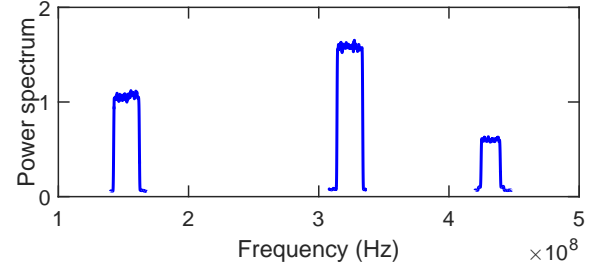
$$\text{CRB}(\boldsymbol{\alpha}) = \mathbf{\Omega}^{-1}. \quad (78)$$



(a) True and estimated carrier frequencies and DoAs.



(b) Original power spectra of sources.



(c) Estimated power spectra of sources.

Fig. 4. True and estimated carrier frequencies, DoAs, and power spectra of sources, SNR = 5dB.

### VIII. SIMULATION RESULTS

In this section, we carry out experiments to illustrate the performance of our proposed method. In our simulations, we set  $f_{\text{nyq}} = 1\text{GHz}$ . The distance between two adjacent antennas,  $d$ , is set equal to  $d = 0.8 \times C/f_{\text{nyq}}$  in order to meet the condition in Assumption A6. The number of antennas is set to  $N = 8$ , and for simplicity, the time delay factors are set as

$$\Delta_n = \begin{cases} 0 \text{ s}, & n = 1, \dots, N/2 \\ 10^{-9} \text{ s}, & n = N/2 + 1, \dots, N \end{cases} \quad (79)$$

With this setup, the condition (6) can be satisfied for  $n = N/2 - 1$ . The signal-to-noise ratio (SNR) is defined as

$$\text{SNR} \triangleq \frac{\mathbb{E}[|s(t)|^2]}{\sigma^2} \quad (80)$$

We first consider the case in which  $K = 3$  uncorrelated, wide-sense stationary sources spreading over the wide frequency band  $(0, 500]\text{MHz}$  impinge on a ULA of  $N$  antennas. The DoAs of these three sources are given respectively by  $\theta_1 = 2.051$ ,  $\theta_2 = 1.447$ , and  $\theta_3 = 0.361$ . The carrier frequencies and bandwidths associated with these sources are set to  $f_1 = 152\text{MHz}$ ,  $f_2 = 323\text{MHz}$ ,  $f_3 = 432\text{MHz}$ ,  $B_1 = 20\text{MHz}$ ,  $B_2 = 20\text{MHz}$ , and  $B_3 = 15\text{MHz}$ . The complex baseband

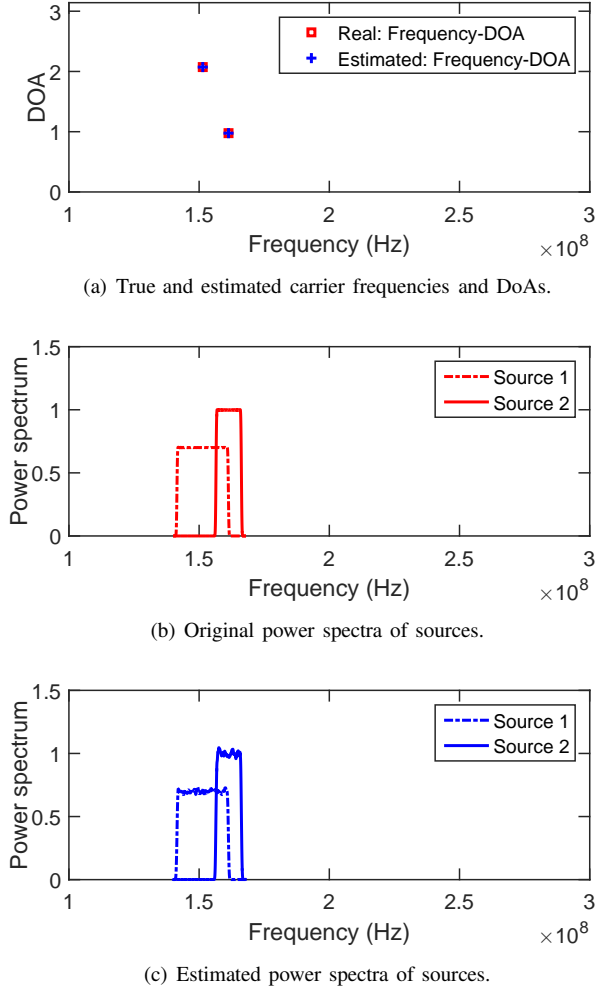


Fig. 5. Estimated carrier frequencies, DoAs and power spectra for sources that have partial spectral overlap, SNR = 20dB.

signals are generated by passing the complex white Gaussian noise through low-pass filters with different cutoff frequencies. Also, the number of data samples used for calculating the correlation matrices is set to  $N_s = 10^5$ . The sampling rate  $f_s$  is chosen to be  $f_s = 28\text{MHz}$ , which is slightly higher than the minimum sampling rate  $f_s \geq B = \max\{B_1, B_2, B_3\}$  required for perfect recover of the power spectrum of the wide frequency band. The SNR is set to 5dB. Fig. 4(a) shows the true (marked with ‘ $\square$ ’) and the estimated (marked with ‘+’) carrier frequencies and DoAs for the three sources. We can see that the estimated carrier frequencies and DoAs coincide with the groundtruth well. Fig. 4(b) and Fig. 4(c) respectively depict the original power spectrum and the estimated power spectrum of the wide frequency band. It can be observed that our proposed method, even with a low SNR and a sampling rate far below the Nyquist rate, is able to accurately identify the locations of the occupied bands.

Next, we examine the scenario where frequency bands of the narrowband sources overlap each other. Set  $K = 2$ . The DoAs of these two sources are given respectively by  $\theta_1 = 2.064$  and  $\theta_2 = 0.968$ . The carrier frequencies and bandwidths associated with these two sources are set to  $f_1 = 151.36\text{MHz}$ ,  $f_2 =$

$161.36\text{MHz}$ ,  $B_1 = 20\text{MHz}$ , and  $B_2 = 10\text{MHz}$ . The power spectra associated with the two sources are shown in Fig. 5(b), from which we can see that the two sources partially overlap in the frequency domain. The number of data samples  $N_s$  and the sampling rate  $f_s$  remain the same as in the previous example. The SNR is set to 20dB. The estimated carrier frequencies, DoAs, and the power spectra of the two sources are plotted in Fig. 5(a) and Fig. 5(c). We see that our proposed method works well for sources with partially overlapping frequency bands. This example shows that our proposed method not only can perform wideband spectrum sensing, but also has the ability to blindly separate power spectra of sources that have partial spectral overlap.

To better evaluate the performance of our proposed method, we calculate the mean square errors (MSEs) for the following sets of parameters

$$\begin{aligned} \text{MSE}(\psi) &= \sum_{k=1}^K |\psi_k - \hat{\psi}_k|^2 \\ \text{MSE}(\xi) &= \sum_{k=1}^K |\xi_k - \hat{\xi}_k|^2 \\ \text{MSE}(\theta) &= \sum_{k=1}^K |\theta_k - \hat{\theta}_k|^2 \end{aligned}$$

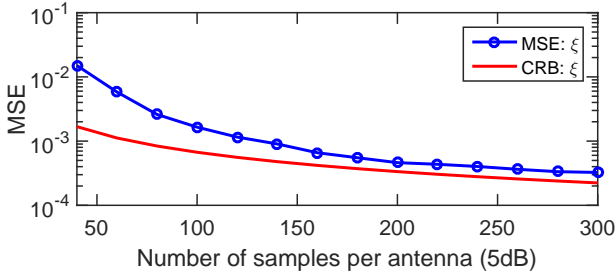
Recalling that in our analysis, instead of concerning  $\{\theta_k, \omega_k\}$ , we define two new parameters  $\xi_k \triangleq \omega_k \tau_k$  and  $\psi_k \triangleq \omega_k / c$  and derive the CRB for  $\{\xi_k, \psi_k\}$  in order to avoid the numerical instability issue. The MSEs of the sets of parameters  $\{\xi_k, \psi_k\}$  are also included to compare with their associated CRB results. The estimation accuracy of the carrier frequencies is quantified by the normalized mean square error (NMSE) defined as

$$\text{NMSE}(\omega) = \sum_{k=1}^K \frac{|\omega_k - \hat{\omega}_k|^2}{|\omega_k|^2}$$

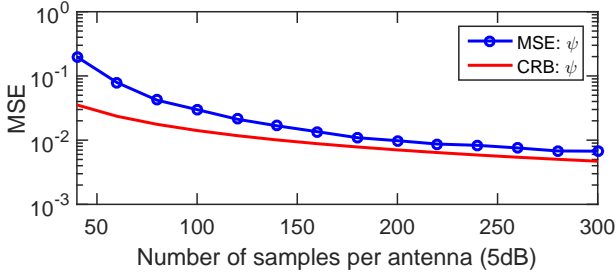
In this example, we set the number of sources  $K = 2$ . The parameters associated with these two sources are given as:  $f_1 = 152\text{MHz}$ ,  $f_2 = 437\text{MHz}$ ,  $B_1 = 126\text{KHz}$ ,  $B_2 = 63\text{KHz}$ ,  $\theta_1 = \pi/4$ , and  $\theta_2 = \pi/3$ . The sampling rate is set to  $f_s = 1.26\text{MHz}$ . Fig. 6 and Fig. 7 depict the MSEs/NMSEs of respective sets of parameters vs. the number of samples  $N_s$ , where we set SNR = 5dB and SNR = 15dB, respectively. MSE/NMSE results are averaged over 1000 independent runs, where the baseband complex source signals are randomly generated for each run. We see that our proposed method can achieve an estimation accuracy close to the CRBs by using only a small number of data samples, e.g.  $N_s = 200$ . In Fig. 8, we plot the MSEs/NMSEs of different sets of parameters as a function of the SNR, where  $N_s = 300$  data samples are used. We see that under a moderately high SNR, say, SNR = 15dB, our proposed method attains an accurate estimate of the DoAs/carrier frequencies with the MSE (NMSE) as low as  $10^{-4}$ .

## IX. CONCLUSIONS

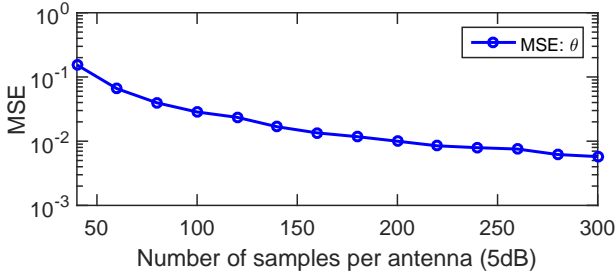
We considered the problem of joint wideband spectrum sensing and DoA estimation in this paper. To overcome



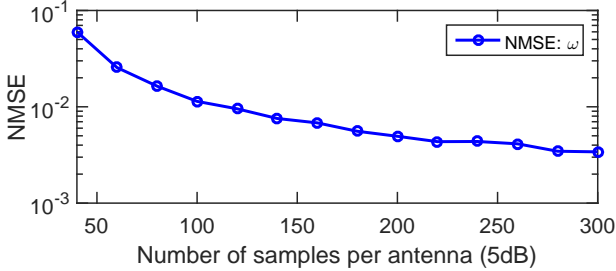
(a)



(b)

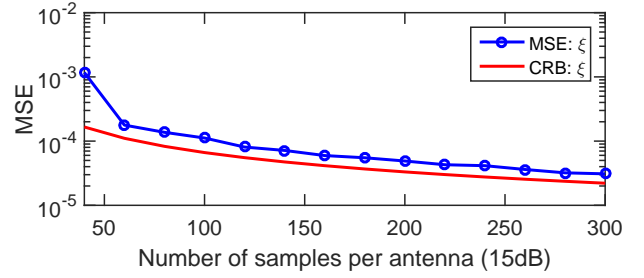


(c)

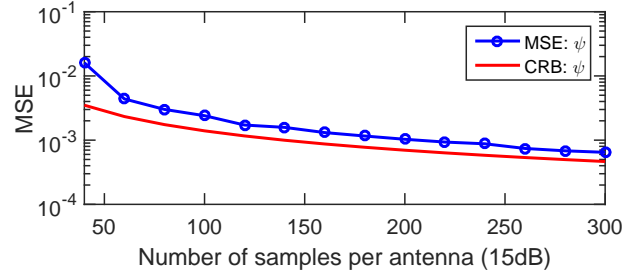


(d)

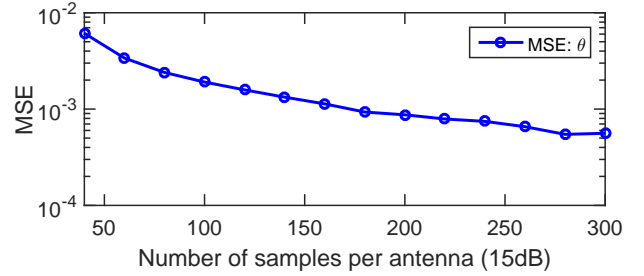
Fig. 6. MSEs and NMSE vs. the number of samples per antenna, where  $N = 8$  and  $\text{SNR} = 5\text{dB}$ .



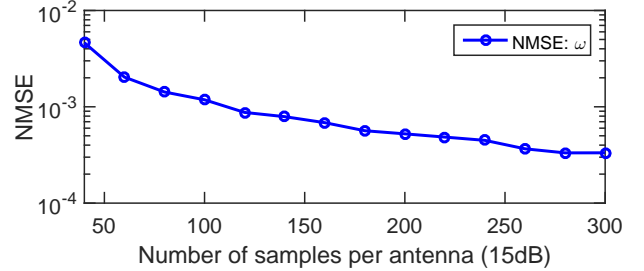
(a)



(b)



(c)



(d)

Fig. 7. MSEs and NMSE vs. the number of samples per antenna, where  $N = 8$  and  $\text{SNR} = 15\text{dB}$ .

the sampling rate bottleneck, we proposed a phased-array based sub-Nyquist sampling architecture (termed as PASSAT) that is simpler in structure and easier for implementation as compared with existing sub-Nyquist receiver architectures. Based on the proposed receiver architecture, we developed a CP decomposition-based method for joint DoA, carrier frequency, and power spectrum estimation. The conditions for exact recovery of the parameters and the power spectrum were analyzed. Our analysis suggests that the perfect recovery condition for our proposed method is mild: to recover the power spectrum of the wide frequency band, we only need

the sampling rate to be greater than the bandwidth of the narrowband source signal which has the largest bandwidth among all sources. In addition, even for the case where sources have partial spectral overlap, our proposed method is still able to extract the DoA, carrier frequency, and the power spectrum associated with each source signal. CRB analysis for our estimation problem was also carried out. Simulation results show that our proposed method, with only a small number of data samples, can achieve an estimation accuracy close to the associated CRBs.

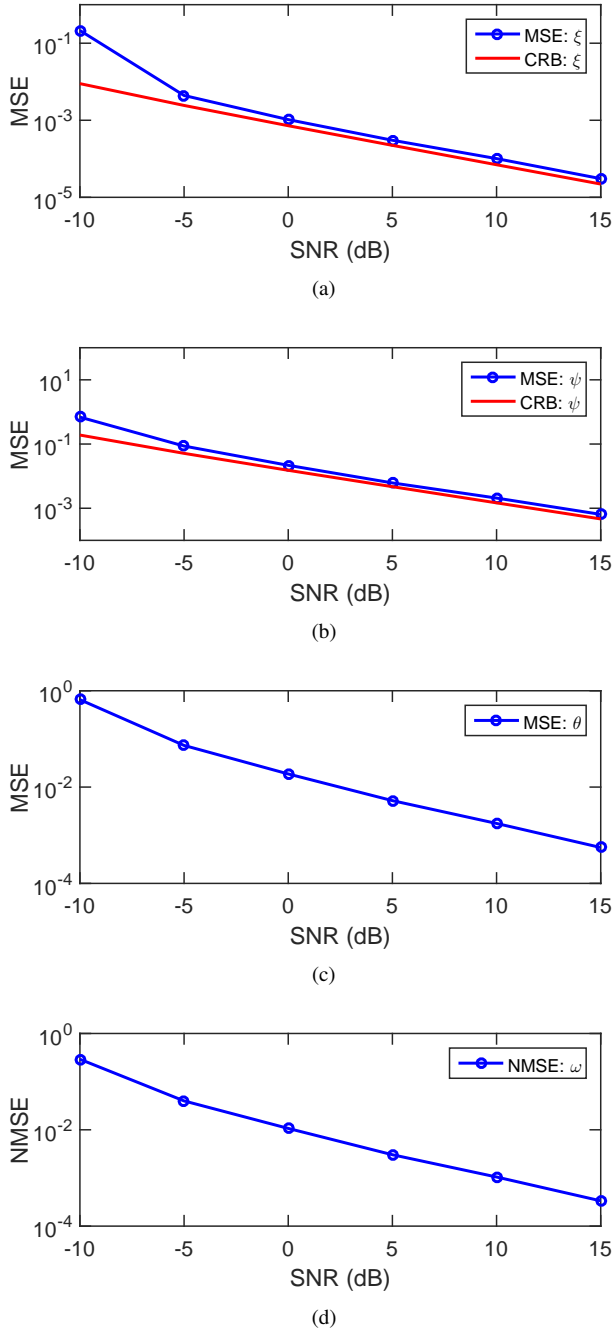


Fig. 8. MSEs and NMSE vs. SNR (dB), where  $N = 8$  and  $N_s = 300$ .

## REFERENCES

- [1] E. Axel, G. Leus, E. G. Larsson, and H. V. Poor, "Spectrum sensing for cognitive radio: State-of-the-art and recent advances," *IEEE Signal Processing Magazine*, vol. 29, no. 3, pp. 101–116, May 2012.
- [2] H. Sun, A. Nallanathan, C.-X. Wang, and Y. Chen, "Wideband spectrum sensing for cognitive radio networks: a survey," *IEEE Wireless Communications*, vol. 20, no. 2, pp. 74–81, Apr. 2013.
- [3] M. Mishali and Y. C. Eldar, "Blind multiband signal reconstruction: Compressed sensing for analog signals," *IEEE Trans. Signal Processing*, vol. 57, no. 3, pp. 993–1009, Mar. 2009.
- [4] —, "From theory to practice: Sub-Nyquist sampling of sparse wideband analog signals," *IEEE J. Sel. Topics Signal Process.*, vol. 4, no. 2, pp. 375–391, Apr. 2010.
- [5] M. Mishali, Y. C. Eldar, O. Dounaevsky, and E. Shoshan, "Xampling:

- Analog to digital at sub-Nyquist rates," *IET Circuits, Devices and Systems*, vol. 5, no. 1, pp. 8–20, Jan. 2011.
- [6] M. Wakin, S. Becker, E. Nakamura, M. Grant, E. Sovero, D. Ching, J. Yoo, J. Romberg, A. Emami-Neyestanak, and E. Candès, "A nonuniform sampler for wideband spectrally-sparse environments," *IEEE Journal on Emerging and Selected Topics in Circuits and Systems*, vol. 2, no. 3, pp. 516–529, Sept. 2012.
- [7] E. Candès, J. Romberg, and T. Tao, "Robust uncertainty principles: exact signal reconstruction from highly incomplete frequency information," *IEEE Trans. Information Theory*, vol. 52, no. 2, pp. 489–509, Feb. 2006.
- [8] D. L. Donoho, "Compressive sensing," *IEEE Trans. Information Theory*, vol. 52, no. 4, pp. 1289–1306, Apr. 2006.
- [9] D. D. Ariananda and G. Leus, "Compressive wideband power spectrum estimation," *IEEE Trans. Signal Processing*, vol. 60, no. 9, pp. 4775–4789, Sept. 2012.
- [10] C.-P. Yen, Y. Tsai, and X. Wang, "Wideband spectrum sensing based on sub-Nyquist sampling," *IEEE Trans. Signal Processing*, vol. 61, no. 12, pp. 3028–3040, June 2013.
- [11] D. Cohen and Y. C. Eldar, "Sub-Nyquist sampling for power spectrum sensing in cognitive radios: A unified approach," *IEEE Trans. Signal Processing*, vol. 62, no. 15, pp. 3897–3910, Aug. 2014.
- [12] M. D. Zoltowski and C. P. Mathews, "Real-time frequency and 2-D angle estimation with sub-Nyquist spatio-temporal sampling," *IEEE Trans. Signal Processing*, vol. 42, no. 10, pp. 2781–2794, Oct. 1994.
- [13] S. Stein, O. Yair, D. Cohen, and Y. C. Eldar, "Joint spectrum sensing and direction of arrival recovery from sub-Nyquist samples," in *IEEE International Workshop on Signal Processing Advances in Wireless Communications*, Stockholm, Sweden, 2015, pp. 331–335.
- [14] A. N. Lemma, A.-J. van der Veen, and E. F. Deprettere, "Joint angle-frequency estimation using multi-resolution ESPRIT," in *IEEE International Conference on Acoustics, Speech, and Signal Processing*, Seattle, Washington, USA, 1998, pp. 1957–1960.
- [15] —, "Analysis of joint angle-frequency estimation using ESPRIT," *IEEE Trans. Signal Processing*, vol. 51, no. 5, pp. 1264–1283, May 2003.
- [16] D. D. Ariananda and G. Leus, "Compressive joint angular-frequency power spectrum estimation," in *IEEE European Signal Processing Conference*, Marrakech, Morocco, 2013, pp. 1–5.
- [17] A. A. Kumar, S. G. Razul, and C.-M. S. See, "An efficient sub-Nyquist receiver architecture for spectrum blind reconstruction and direction of arrival estimation," in *IEEE International Conference on Acoustics, Speech, and Signal Processing*, Florence, Italy, 2014, pp. 6781–6785.
- [18] —, "Spectrum blind reconstruction and direction of arrival estimation at sub-Nyquist sampling rates with uniform linear array," in *IEEE International Conference on Digital Signal Processing*, Singapore, 2015, pp. 670–674.
- [19] S. S. Ioushua, O. Yair, D. Cohen, and Y. C. Eldar, "CaSCADE: Compressed carrier and DOA estimation," *IEEE Trans. Signal Processing*, vol. 65, no. 10, pp. 2645–2658, May 2017.
- [20] T. G. Kolda and B. W. Bader, "Tensor decompositions and applications," *SIAM review*, vol. 51, no. 3, pp. 455–500, 2009.
- [21] A. Lavrenko, F. Römer, S. Stein, D. Cohen, G. D. Galdo, R. S. Thomä, and Y. C. Eldar, "Spatially resolved sub-Nyquist sampling of multiband signals with arbitrary antenna arrays," in *IEEE International Workshop on Signal Processing Advances in Wireless Communications*, Edinburgh, UK, 2016, pp. 1–5.
- [22] J. A. Bazerque, G. Mateos, and G. B. Giannakis, "Rank regularization and bayesian inference for tensor completion and extrapolation," *IEEE Trans. Signal Processing*, vol. 61, no. 22, pp. 5689–5703, November 2013.
- [23] P. Rai, Y. Wang, S. Guo, G. Chen, D. Dunson, and L. Carin, "Scalable Bayesian low-rank decomposition of incomplete multiway tensors," in *Proc. of the 31st Inter. Conf. on Mach. Learning (ICML-14)*, vol. 32, Beijing, China, 2014, pp. 1800–1808.
- [24] Q. Zhao, L. Zhang, and A. Cichocki, "Bayesian CP factorization of incomplete tensors with automatic rank determination," *IEEE Trans. Pattern Anal. Mach. Intell.*, vol. 37, no. 9, pp. 1751–1763, Sept. 2015.
- [25] J. B. Kruskal, "Three-way arrays: rank and uniqueness of trilinear decompositions, with application to arithmetic complexity and statistics," *Linear Algebra and its Applications*, vol. 18, no. 2, pp. 95–138, 1977.
- [26] A. Stegeman and N. D. Sidiropoulos, "On Kruskal's uniqueness condition for the Candecomp/Parafac decomposition," *Linear Algebra and its Applications*, vol. 420, no. 2–3, pp. 540–552, Jan. 2007.
- [27] R. A. Harshman, "Determination and proof of minimum uniqueness conditions for PARAFAC1," *UCLA Working Papers in Phonetics*, no. 22, pp. 111–117, 1972.

- [28] S. M. Kay, *Fundamentals of Statistical Signal Processing: Estimation Theory*. Upper Saddle River, NJ: Prentice Hall, 1993.
- [29] P. Stoica and A. Nehorai, "Performance study of conditional and unconditional direction-of-arrival estimation," *IEEE Trans. Acoust., Speech, Signal Processing*, vol. 38, no. 10, pp. 1783–1795, Oct. 1990.
- [30] P. Stoica, E. G. Larsson, and A. B. Gershman, "The stochastic CRB for array processing: a textbook derivation," *IEEE Signal Processing Lett.*, vol. 8, no. 5, pp. 148–150, May 2001.